Virtual Modeling and Numerical Simulation of Aneurysms and Stenoses

Rodrigo L. S. Silva, Eduardo Camargo, Pablo Javier Blanco, Márcio Pivello, Rául A. Feijóo
National Laboratory for Scientific Computation
Hemodynamic Modeling Laboratory
Petrópolis, Rio de Janeiro, Brazil
{rodrigo,camargo,pjblanco,pivello,feij}@lncc.br

Abstract

This paper presents a first approach to model and simulate hemodynamic pathologies, based on geometrical singularities, such as Aneurysms and Stenoses. The techniques described in this work allow the specialist to add these pathologies based on parameterized geometries or over real arterial geometries, usually obtained via segmentation techniques from medical images. The relative position of the pathology on the artery can be interactively changed with the aim of obtaining a better understanding of the disease.

1. Introduction

The increase of cardiovascular diseases in the last years has motivated the development of, for instance, computational techniques in order to aid their treatment. The complexity of these surgical interventions is notably growing in the last years due the fast advances in modern medicine. Some cardiovascular diseases, such as arterioscleroses and cerebral aneurysms, are reported to depend on hemodynamic factors, particularly on the characteristics of the wall shear stress induced by blood flow [1]. With the purpose of joining tools to aid the treatment of these diseases a computational environment called HeMoLab was created [6]. HeMoLab is a computer system that allows the creation of patient-oriented models of the human cardiovascular system and also the numerical simulation within a unified framework.

The 3D modeling of the human cardiovascular system (HCS) aims to study with a high level of detail the hemodynamic features of the blood flow and how those features are modified when, for instance, a surgical planning is devised over such system. Any part of the arterial network can be represented in details by using patient-specific data (such as medical images) of the arterial district of interest. Particular cases, like the presence of geometric singularities (aneurysm, stenoses, bifurcations and so on) can be simulated in order to study local changes in the blood flow structure and used to retrieve a more complete quantitative information.

A complete simulation is composed by the reconstruction of the geometrical data through medical imaging systems (Magnetic Resonance Imaging and Computed Tomography), determination of boundary conditions and mechanical properties of the blood and arterial walls of the selected area and finally the computation of an approximate solution of the problem.

This paper presents an interactive system to create and simulate virtual aneurysms and stenoses over parameterized geometrical structures and patient-based arteries. This interactivity allows the user to simulate several conditions and analyze the numerical results graphically using visualization techniques such as stream-lines, stream-tubes, warping techniques for the velocity field, etc.

The tool developed in this paper was integrated into the HeMoLab system that, in turn, is supported by the ParaView architecture [11]. ParaView is a point-and-click 3D scientific visualization system that allows for most of the common visualization techniques (isocontouring, volume rendering) on structured and unstructured grids. Its implementation uses distributed memory parallelism, and is focused on visual data analysis of large scientific datasets. It is an open-source, multi-platform visualization application, and supports distributed computation models to process large datasets. It has an open, flexible, and intuitive user interface and an extensible architecture based on the Visualization Toolkit (VTK) [19].

The remainder of this work is organized as follows: Section 2 presents a brief survey of some works related to computer modelling of the cardiovascular system. In Section 3, the algorithm for the generation of aneurysms and stenoses

is detailed, whereas mathematical modelling and numerical approximation of the physical phenomena involved are described in Sections 4 and 5, respectively. Results obtained after simulating the flow inside a patient-specific artery modified by the tools presented here are shown in Section 6, and some concluding remarks are listed in Section 7.

2. Related Works

Cardiovascular diseases are one of the leading causes of death, morbidity, and invalidity in the world and several works have been conducted in order to prevent, treat and/or diagnose those pathologies. Some work oriented to the treatment, visualization, simulation and diagnosis of stenoses and aneurysms can be viewed in [9, 10, 12, 14].

For instance, in [7] a training system developed with medical purposes was proposed. The system enables the instructor to generate specific cases for analysis, allowing to gain insight not only in the basic feature of searching and stenosis evaluation processes, but also about the importance of the correct viewpoint of acquisition within the environment.

The authors of [8] propose an algorithm that decomposes the patterns of 3D unsteady blood flow into behavioral components to reduce the visual complexity while retaining the structure and information of the original data. The key point of the algorithm is to enable the visualization of large simulated data sets avoiding visual clutter and ambiguity.

This paper differs from these previous approaches by adding a friendly interface to enable the interactive positioning of the aneurysm or the selection of the cut area in the case of a stenosis. Also, algorithms to join two or more meshes with a different resolution were implemented. This feature allows the user to study diverse cases in an interactive and intuitive manner.

3. Modeling Aneurysms and Stenoses

The main feature of the tool proposed in this paper is the ability to easily merge two meshes so as to create new geometries maintaining the correct topology. A friendly interface was designed to enable an interactive positioning of the geometrical region to be added or removed in the case of aneurysm or stenosis, respectively.

Basically, the system provides a sphere widget (Figure 1.a) to be added on a given region to create an aneurysm, or use this sphere to remove a portion of the arterial district to create a stenosis.

In Figure 1.b, the geometry of the widget was added to, in this case, a parameterized carotid bifurcation to create a virtual aneurysm. The same widget can be translated to another position as can be seen in 1.c, where it is employed to simulate the presence of a stenosis.

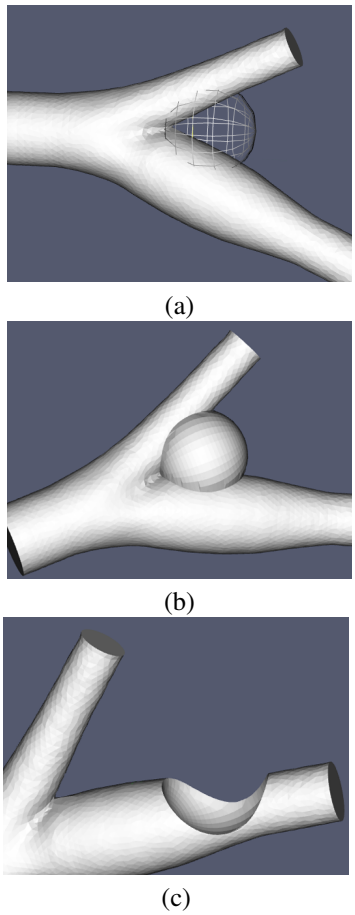

(a) (b) (c)

Figure 1. In (a), sphere widget used to model aneurysms and stenoses. In (b) a virtual aneurysm and in (c) a virtual stenosis. Both examples without geometry smoothing.

Finally, Figure 2 shows the result of the altered geometry presented in Figure 1.c after some geometry smoothing.

3.1 Merging surfaces

One of the major problems of creating the pathologies mentioned above was to merge different meshes while preserving the consistency of the topology, connectivity and point sharing. To solve this problem the following steps were adopted:

- set the sphere widget in the right position;
- clip the main surface with the widget;
- find boundary triangles on the clipped area;

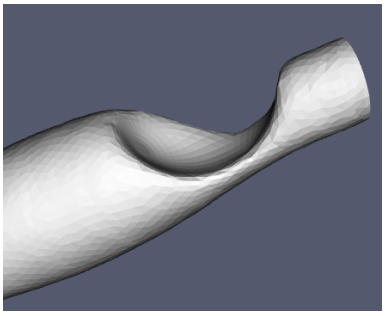

Figure 2. Filtered representation of the Figure 1.c.

- find the intersection between the clipped surface and the sphere widget;
- merge the two surfaces discarding the unused triangles on the sphere and the ones over the original geometry;

The resolution used in the geometrical representation of the sphere is also an issue. The ideal case is when the resolution of the sphere is the same as the resolution of the main surface. In this situation, joining the two meshes is easier, because the number of points to be joined in the clipped surface and the sphere is similar. Even when the resolution is similar, the number of the points in both surfaces generally is not the same. To solve this problem, an algorithm to *sew* the two meshes was developed. Basically, two points of each geometrical entity are used as seeds. The first point is chosen arbitrarily and the second point is found by computing the smallest Euclidean distance between the first point and all of the points of the other board. Based on these two points, a direction is selected and the sewing process starts, as illustrated in Figure 3.a. Since the two surfaces have different numbers of points in the region of intersection, one single point of one surface can be linked by edges with many other points of the other surface (Figure 3.b). As said, a criterion of proximity based on Euclidean distance was used to perform that linking.

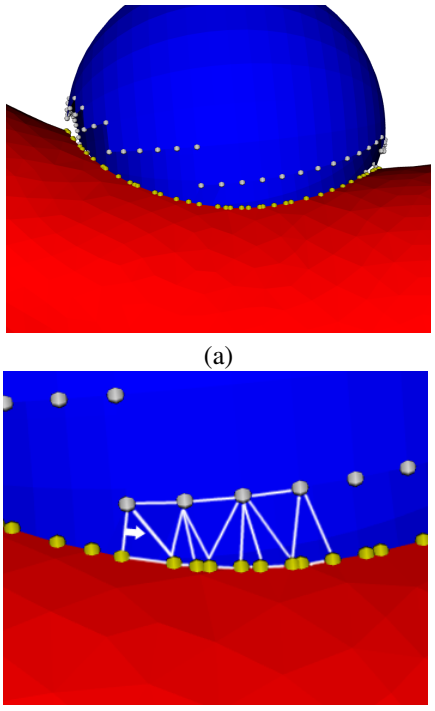

(a)

(b)

Figure 3. In (a) the points of the surface (yellow) and the points of the sphere (gray). The white arrow is over the edge linking the two seed points in (b) where the beginning of the sewing process is illustrated. The white arrow also shows the sewing direction.

3.2 Removing malformed elements

The generation of high quality meshes is a fundamental step towards the resolution of a problem via an approximate technique such as the finite element method. The techniques described above generate a surface with the right topology but do not guarantee the quality of the mesh. Some special algorithms were developed to handle malformed triangles, e.g., needle-like triangles (Figure 4.a), or tiny triangles that have a much smaller area than the average element area in the surrounding region. (Figure 4.b).

Basically a good algorithm should remove those malformed elements maintaining the right connectivity with the surrounding elements. A needle triangle has always one neighbor that must be also removed, unless its smaller edge is located on a non-shared boundary. In any other case, this neighbor shares the smaller edge with the needle triangle as illustrated in Figure 4.c. A small triangle, when removed, forces the removal of all surrounding triangles (usually needles) as pictured in 4.d.

These algorithms were implemented in ParaView and can be interactively used through an user-friendly interface. Needles are identified by a user-set threshold angle that defines the minimum angle allowed in an element. All the elements that have angles bellow the threshold are then highlighted, and the user can take them out from the mesh. Tiny elements are also defined by a threshold value, which represents now a percentage of the average area in the mesh. Elements bellow the threshold are highlighted and, again, the user can erase them. Details and examples about the algorithms described above can be found in [13].

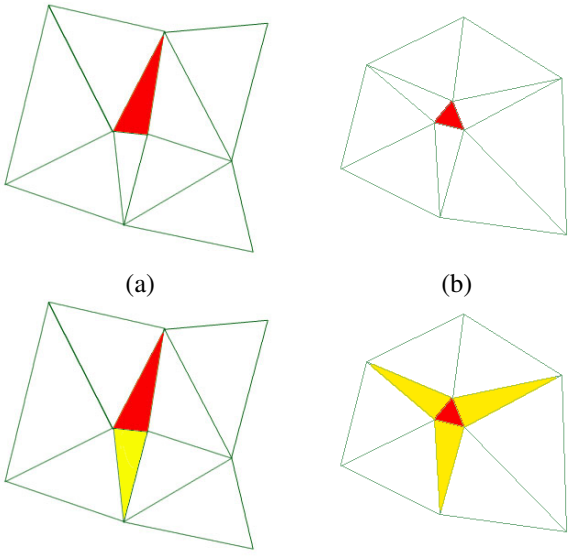

Figure 4. Red Triangles represent malformed elements like needle (a) and small triangles (b). In (b) and (c) the neighbors in yellow are triangles marked to be removed.

4 Mathematical Model of the coupled 3D – 1D blood flow simulation

Blood flow simulation is performed with a coupled 3D – 1D model of the arterial system, which consists in embedding a 3D model of an artery in a simplified 1D model of the arterial system. Inlets and outlets of the 3D model are coupled with their respective counterparts in the 1D model, such that no 3D boundary condition is necessary. The main advantage of using 3D–1D coupled models is that they behave as a unique system, avoiding the need for measurements that would be required when employing standalone 3D models. The boundary conditions over the inlets-outlets of the 3D region are accounted for the own solution of the entire problem. In other words, it can be understood in the following way: the 1D model feeds the 3D model with certain conditions and viceversa. On the other hand, the boundary conditions needed are the heart inflow boundary condition that represents the heart ejection and the Windkessel terminals, which are used to simulate the peripheral beds not included in the model. Therefore, once the 1D model is calibrated and validated, any artery which is present in the model may be replaced by a detailed 3D counterpart that is able to yield richer qualitative and quantitative results about the flow patterns in that region. This is particularly useful when studying pathologies such as aneurysm, stenoses, etc. which are phenomena based on local factors.

The governing equations were derived based on a variational formulation for the coupling of kinematically incompatible models, in this case 3D-1D flow models in compliant vessels [3]. The associated Euler equations for a Newtonian fluid when coupling a 1D domain Ω_{1D} with a 3D region Ω_{3D} through a coupling interface Γ_c, and considering the ALE (Arbitrary Lagrangian Eulerian) formulation over Ω_{3D}, are the following:

$$\rho A\frac{\partial \bar{u}}{\partial t}+\rho A\bar{u}\frac{\partial \bar{u}}{\partial z}=-A\frac{\partial \bar{p}}{\partial z}-8\pi\mu\bar{u}+f^z \quad \text{in } \Omega_{1D}\times(0,T) \tag{1}$$

$$\rho\frac{\partial \mathbf{u}}{\partial t}\bigg|_{\mathbf{Y}}+\rho\nabla\mathbf{u}\left(\mathbf{u}-\mathbf{w}\right)=-\nabla p+\mu\Delta\mathbf{u}+\mathbf{f} \quad \text{in } \Omega_{3D}\times(0,T) \tag{2}$$

$$\frac{\partial A}{\partial t}+\frac{\partial\left(A\bar{u}\right)}{\partial z}=0 \quad \text{in } \Omega_{1D}\times(0,T) \tag{3}$$

$$\nabla\cdot\mathbf{u}=0 \quad \text{in } \Omega_{3D}\times(0,T) \tag{4}$$

$$\left(-p\mathbf{I}+2\mu\boldsymbol{\varepsilon}(\mathbf{u})\right)\mathbf{n}_1=-\bar{p}\mathbf{n}_1 \quad \text{on } \Gamma_c\times(0,T) \tag{5}$$

$$A_c\bar{u}=\int_{\Gamma_c}\mathbf{u}\cdot\mathbf{n}_1\,d\Gamma \quad \text{on } \Gamma_c\times(0,T) \tag{6}$$

Where $\mathbf{n}_1$ is the unit outward normal to domain Ω_{1D} over the coupling interface Γ_c. In equations 1 and 3, which represent the 1D model, $\bar{u}$, $\bar{p}$ are the mean velocity and pressure values, ρ is the blood density, μ is the dynamic viscosity, A denotes the cross sectional area, $Q=A\bar{u}$ is the flow rate and z is the axial coordinate. Equations 2 and 4 represent the 3D model, $\mathbf{u}$ is the blood velocity, $\mathbf{w}$ is the domain velocity of change consistent with the ALE framework, while p is the blood pressure. Equation 5 stands for the continuity of the traction vector at Γ_c (the coupling interface between the 3D and 1D models), while expression 6 is the counterpart of the mass conservation.

The wall movement is modelled according to the independent ring model [4], and its equations are stated bellow:

$$\bar{p}=\bar{p}_0+\frac{E\pi R_0h_0}{A}\left(\sqrt{\frac{A}{A_0}}-1\right)+ +\frac{k\pi R_0h_0}{A}\frac{1}{2\sqrt{A_0A}}\frac{\mathrm{d}A}{\mathrm{d}t} \quad \text{in } \Omega_{1D}\times(0,T) \tag{7}$$

$$p=p_0+\frac{Eh}{R_0^2}\zeta+\frac{kh}{R_0^2}\frac{\mathrm{d}\zeta}{\mathrm{d}t} \quad \text{in } \Gamma_w\times(0,T) \tag{8}$$

This is a rather simplified model of the structural behavior of the arterial wall, but serves to take into account the arterial compliance. The deformation of the domain Ω_{3D} is

accounted for through a Laplacian problem, as stated bellow:

$$\nabla^2 \mathbf{d} = 0 \qquad \text{in} \qquad \Omega_{3D} \times (0, T) \tag{9}$$

Since it is a small amplitude movement, no remeshing is performed. Instead, equation 9 is used in order to extend the wall movement to the interior of Ω_{3D}, and $\mathbf{d}|_{\Gamma_w} = \zeta \mathbf{n}$ is the wall displacement, where ζ is the scalar field that denotes the displacement of the wall in the normal direction, given by $\mathbf{n}$, that is obtained from equation 8. Finally, it is $\mathbf{w} = \frac{\partial \mathbf{d}}{\partial t}$. Refer to [3] for a further theoretical account about the coupling of 3D-1D blood flow models.

5 Numerical Approximation

In this section the numerical aspects of this work are briefly described. In this sense, details concerning the numerical techniques applied, the setting of the model regarding boundary conditions, the 3D geometry and the 1D arterial network topology are given.

5.1 Geometry Segmentation and Mesh Generation

The first step to obtain a 3D geometry of the artery is to apply an image segmentation technique to it. The output of this process is a 3D geometry representing the chosen region, which is then used as an input to a mesh generation software.

Image Segmentation consists in identifying and isolating a region of interest in an image data set, be it 2D or 3D. In this paper a voxel grow approach was used, which consists in finding the neighbors of a given point based on its neighborhood connectivity and on its color level (or level, for short). Starting from a manually handled seed point and a bandwidth for the level, each neighbor of the point, if its level is within this bandwidth, is added to the output data set. The process is repeated recursively to each point added to this data set until the whole image has been analyzed. Also, multiple seeds with multiple bandwidths may be used. In this case, the seed point was chosen within the artery to be analyzed and the external contour of the output data set determined the geometry of its 3D model, which was used as input for the mesh generation process. For more information about the image segmentation process and other related topics refer to [5] and references therein. The surface obtained after processing the image must be properly manipulated to generate a high-quality mesh. This manipulation involves smoothing, addition of nodes, removing needle-like elements among other classical techniques. Once the triangulation of the surface is satisfactory, the volume mesh generation is performed using a Delaunay technique. The algorithms used for both surface and volume mesh generation are detailed in [17, 18].

5.2 Numerical Approximation of the Blood Flow Model

The numerical approximation of the problem is quite classical and we refer again to [3] for further details. The time discretization is performed by means of a single step finite difference method corresponding to a classical θ scheme for both 1D and 3D parts. The spatial discretization is carried out through the finite element method. Variables Q, A, $\bar{p}$ of the 1D model are discretized with $\mathbb{P}_1$ finite elements, while $\mathbf{u}$, p in the 3D model are discretized with $\mathbb{P}_1^B - \mathbb{P}_1$ finite elements. The index B stands for bubble functions for the velocity field according to the mini element formulation [2]. The domain displacement, $\mathbf{d}$, is also approximated with $\mathbb{P}_1$ finite elements, and the reference velocity $\mathbf{w}$ is computed from the displacement by a backward Euler difference scheme. For both 1D and 3D parts, stabilization terms must be included in order to avoid the non–physical oscillating solutions present in standard Galerkin approximations. For the 1D model these terms are incorporated along the characteristics lines and correspond to a Galerkin Least Squares formulation [16]. For the 3D model the stabilization terms correspond to the Streamline Upwind Petrov Galerkin technique with a suitable stabilization parameter [15]. In all cases, nonlinearities are treated with Picard iterations.

6 Results

In order to show the capabilities of the tool described above, we present the results of the flow simulation inside a segment of the right interior carotid artery in two situations: (i): when an aneurysm was added with the tool described before and (ii) when the healthy artery was used in the simulation, for comparison purposes. It was used an SGI Altix 3700 BX2 workstation. This machine consists of 32 Itanium2 1.5 GHz processors with 64 GBRAM. The operational system is SUSE Linux Enterprise Server 9. The numerical solver is written in FORTRAN90 and the HeMoLab system is developed in C++, using the VTK library.

Firstly, Figure 5 shows the interface of the HeMolab system and, specifically, of the tool developed. Figure 6.a shows the geometry for the two cases, while in Figure 7 it is shown the position within the 1D arterial network of the coupling locations (red segment between the green and blue points), Figure 6.b shows details of the mesh in the region of the aneurysm, where it can be seen the smoothness in the transition between the two merged geometries.

The simulation was carried out within two cardiac periods of $T = 0.8$sec each starting from the at-rest situation.

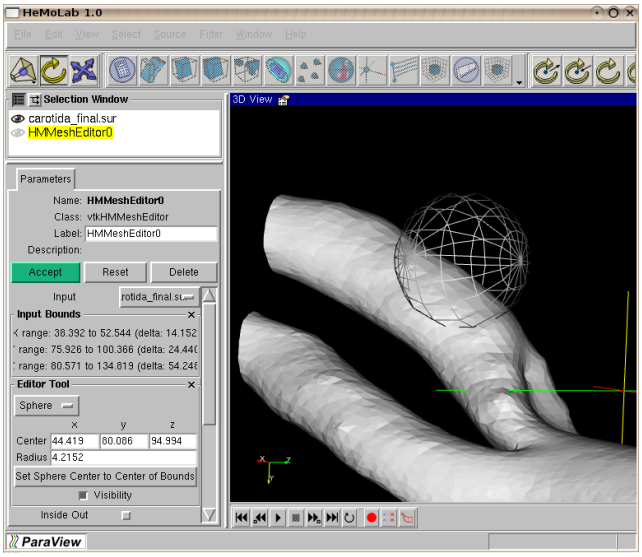

Figure 5. HeMoLab interface. The sphere is interactively positioned over the surface.

Although some time-varying transition should be expected before reaching the time-periodic regime, the main characteristics of the flow patterns are present even when starting the simulation from the at-rest state. The blood flow characteristics are here put into evidence by visualizing the velocity profiles and also some well-known indicators such as the OSI (measures the oscillatory behavior of stresses along a cardiac cycle) and the WSS (measures the mean value of stresses along a cardiac cycle) indexes.

Figures 8.a and 8.d show the flow pattern along the artery for each case at $t = 0.105sec$, with details in the region of the aneurysm. Notice that in the region downstream the aneurysm, both cases led to similar flow patterns and velocity magnitudes. However, after the aneurysm, the velocity is such that higher stresses take place. Also, a natural reduction in the velocity magnitude can be seen inside the aneurysm (see Figures 8.b and 8.e), where more complex flow patterns develop. This region within the aneurysm is also the place where higher values of OSI take place (see Figures 8.c and 8.f): these values were about two times higher in case with aneurysm when compared to the healthy case, while the peak in WSS occurs at the inlet and outlet of the aneurysm where, as it is well-known, the arterial wall is more affected by the blood flow.

Finally, Figure 9 shows the evolution profile of an isosurface of velocity magnitude 20 cm/sec. Here it is possible to appreciate the recirculation pattern of the flow when entering in the aneurysm region.

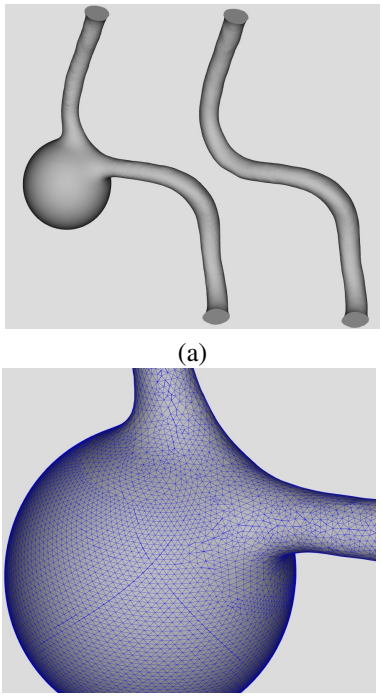

(a)

(b)

Figure 6. In (a) Arterial geometry, with and without aneurysm and in (b) mesh details on the region affected by the aneurysm.

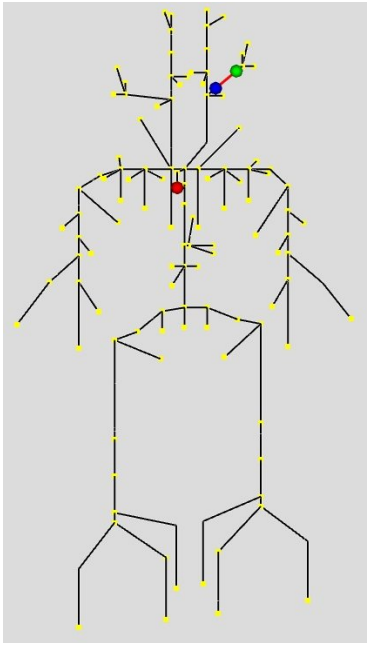

Figure 7. Positioning and coupling points of the 3D arterial district considered within the 1D model.

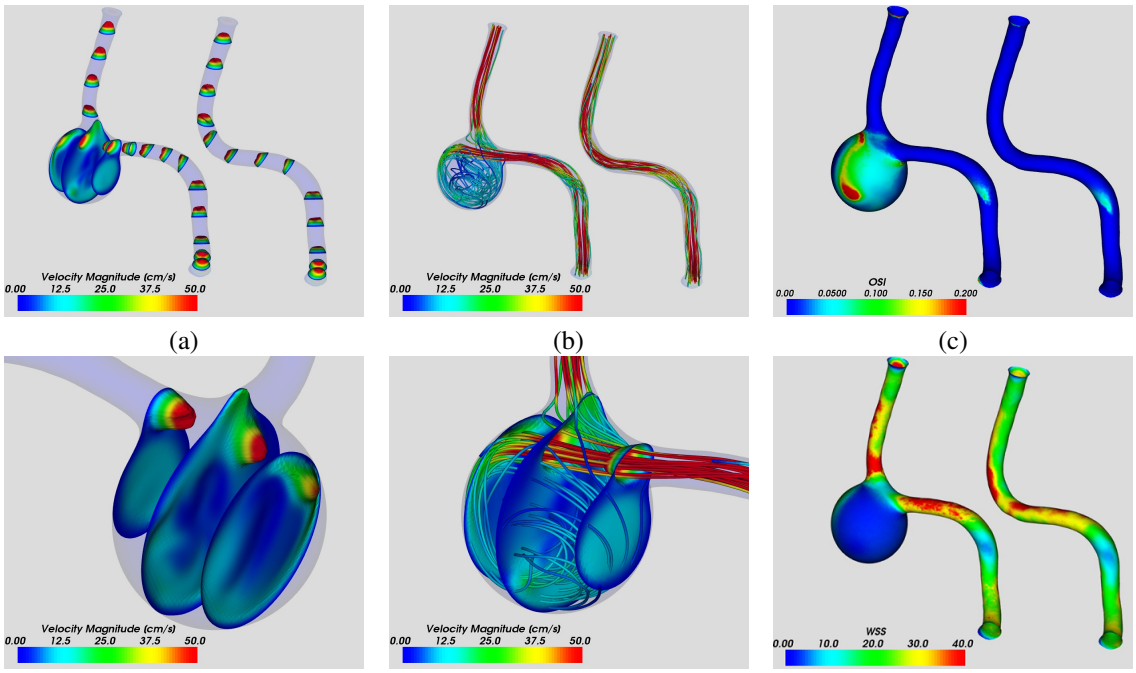

(a) (b) (c)

(d) (e) (f)

Figure 8. (a) and (d) Velocity profiles and in (b) and (e) stream lines along the vessels for T=0.105s. (c) OSI and (f) WSS distribution over the arteries with and without aneurysm.

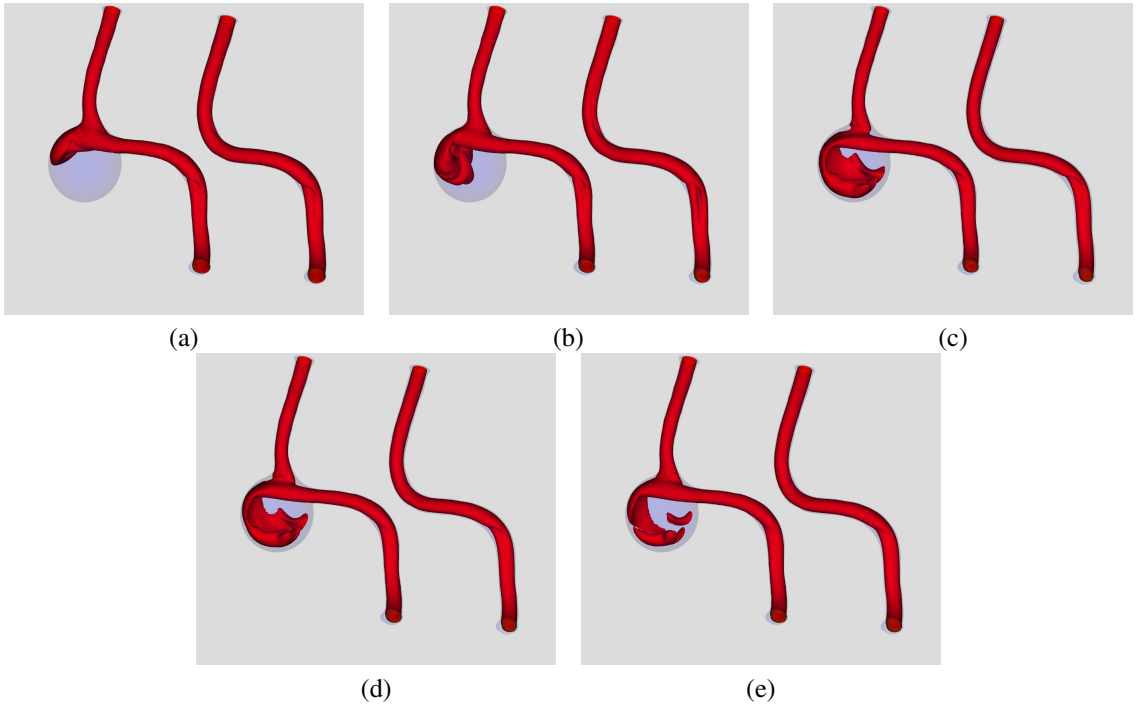

(a) (b) (c)

(d) (e)

Figure 9. Time evolution of an iso surface of velocity magnitude equal to 20 cm/s. From left to right, top to bottom: $t = 0.05$ sec, $t = 0.0625$ sec, $t = 0.0925$ sec, $t = 0.0995$ sec **and** $t = 0.105$ sec.

7. Conclusions

In this work, it has been presented a first approach model and simulate pathologies arising in cardiovascular modeling such as Aneurysms and Stenoses. The geometrical models can be interactively constructed through the manipulation of spherical widgets over a given geometry representing an arterial district of interest.

After the reconstruction of the geometrical singularity that represents the pathology, the system allows in a straightforward way the computation of an approximate solution through the numerical simulation. The numerical results have been then analyzed using several visualization techniques such as stream lines, isosurfaces, arbitrary slices, warping techniques, etc. From the obtained numerical evidences it can be said that this kind of tool permits the the characterization, through diverse numerical indicators, of the altered physical phenomena that occur when different anomalies are present in the cardiovascular system.

Although the present model allows only spherical widgets, this is the first step to model more general and real situations such as elliptic-like perturbations or even free-form perturbations.

References

[1] A.M. Malek, S.L. Alper, and S. Izumo. Hemodynamic shear stress and its role in atherosclerosis. *JAMA*, 282(21):2035–2042, December 1999.

[2] D. Arnold, F. Brezzi, and M. Fortin. A stable finite element for the stokes equations. *Calcolo*, 21(1), 1984.

[3] P. Blanco, R. Feijóo, and S. Urquiza. A unified variational approach for coupling 3D–1D models and its blood flow applications. *Comp. Meth. Appl. Mech. Engrg.*, 196:4391–4410, 2007.

[4] Y. Kivity and R. Collins. Nonlinear fluid–shell interactions: application to blood flow in large arteries. *Int. Sym. Discrete Meth. Engrg.*, pages 476–488, 1974.

[5] I. Larrabide. *Processamento de imagens via derivada topológica e suas aplicações na modelagem e simulação do sistema cardiovascular humano*. PhD thesis, National Laboratory for Scientific Computation, 2007.

[6] I. Larrabide and R. Feijóo. HeMoLab: Laboratório de Modelagem em Hemodinâmica. Technical Report 13/2006, National Laboratory for Scientific Computing, 2006.

[7] I. Lebar Bajec, P. Trunk, D. Oseli, and N. Zimic. Virtual coronary cineangiography. *Computers in Biology and Medicine*, 33(3):293–302, 2003.

[8] D. Lee, D. J. Valentino, G. R. Duckwiler, and W. J. Karplus. Simulation and virtual-reality visualization of blood hemodynamics: the virtual aneurysm. In *Proceedings of SPIE*, volume 4319, pages 465–470, May 2001.

[9] M.R. Harreld. Modeling, Simulation and VR Visualization of Brain Aneurysm Blood Flow. Technical Report 960018, UCLA Computer Science Department, 1996.

[10] M. Oshima. A New Approach to Cerebral Hemodynamics: Patient-Specific Modeling and Numerical Simulation of Blood Flow and Arterial Wall Interaction. *Bulletin for The International Association for Computational Mechanics*, 14:4–9, 2004.

[11] ParaView. http://www.paraview,org.

[12] Y. Sato, T. Araki, and M. Hanayama. A Viewpoint Determination System for Stenosis Diagnosis and Quantification in Coronary Angiographic Image Acquisition. In *IEEE Transaction Medical Imaging*, volume 17, pages 121–137, 1998.

[13] R. Silva, P. Blanco, M. Pivello, and R. Feijóo. Algoritmos para a Homogeneização de Malhas Triangulares. Technical Report 30/2007, National Laboratory for Scientific Computing, 2007.

[14] N. Stergiopulos, D.F. Young, and T.R. Rogge. Computer Simulation of Arterial Flow with Applications to Arterial and Aortic Stenoses. In *Journal of Biomechanics*, volume 25, pages 1477–1488, 1992.

[15] T.J.R. Hughes, L.P. Franca, and M. Mallet. A new finite element formulation for computational fluid dynamics: Vi. convergence analysis of the generalized supg formulation for linear time-dependent multi-dimensional advective-diffusive systems. *Comput. Methods Appl. Mech. Eng.*, 63(1):97–112, 1987.

[16] S. Urquiza, P. Blanco, M. Vénere, and R. Feijóo. Multidimensional modeling for the carotid blood flow. *Comput. Meth. Appl. Mech. Engrg.*, 195:4002–4017, 2006.

[17] M. Vénere. Procedimientos para la generación de mallas tridimensionales de elementos finitos. *Revista internacional de Métodos Numéricos para cálculo y diseño en ingenieria*, 12:3–16, 1996.

[18] M. Vénere. Optimización de la calidad de mallas de elementos finitos mediante cambios localizados de topologia. *Revista internacional de Métodos Numéricos para cálculo y diseño en ingenieria*, 13:3–13, 1997.

[19] VTK - Visualization Toolkit. http://www.vtk.org.